Low-Temperature Dynamics of the 2D Spin-$\frac{1}{2}$ Heisenberg Antiferromagnet: A Quantum Monte Carlo Study

Miloje Makivić
Department of Physics, The Ohio State University, Columbus, Ohio 43210

Mark Jarrell
Department of Physics, University of Cincinnati, Cincinnati, Ohio 45221
(Received 24 May 1991)

We used a combination of quantum Monte Carlo technique and maximum entropy method to calculate the dynamic structure factor of the quantum Heisenberg antiferromagnet. The dynamics is governed by renormalized damped spin waves and we calculate their frequencies and linewidths. The computed spin-wave dispersion is in quantitative agreement with inelastic neutron scattering experiments on La_2CuO_4. The low-energy sector exhibits scaling behavior with the characteristic frequency scale which is inversely proportional to the correlation length.

PACS numbers: 75.10.Jm, 74.70.Hk, 75.40.Mg

Spin dynamics is expected to have a significant role in the understanding of the mechanism for high-temperature superconductivity [1], which is believed to originate from purely electronic degrees of freedom [2]. There is now a consensus [3] that the magnetic degrees of freedom of the undoped compound La_2CuO_4 are well described by the spin-$\frac{1}{2}$ antiferromagnetic Heisenberg model (AFHM):

$$H = J\sum_{\langle ij\rangle} \mathbf{S}_i \cdot \mathbf{S}_j , \tag{1}$$

where $\langle ij\rangle$ goes over all the nearest-neighbor pairs on the square lattice, and $\mathbf{S}_i$ is the spin operator for site i. The exchange coupling J, which sets the energy scale for magnetic excitations, is rather high in this material, and is estimated to be around 1500 K [4–6]. We will measure temperature T in units of J.

There have been significant advances in understanding the static properties of the model, both analytically [7–10] and numerically [5,11–14]. Dynamical simulations of the classical equivalent model were performed recently [15,16]. The situation is quite different regarding dynamical calculations for the quantum model. Accurate numerical results, which are crucial to test the validity of various approximations used in analytical calculations [7,8,16,17], are still lacking. The currently available results based on exact diagonalizations are restricted to small clusters and zero temperature [18].

The present paper reports the first large-scale, nonperturbative study of low-temperature dynamic properties of the quantum AFHM on system sizes large enough to provide an accurate estimate of its properties in the thermodynamic limit. We first compute the dynamic structure factor $S(\mathbf{k},\omega)$ and then use its frequency moments to calculate energies and lifetimes of the elementary excitations (spin waves). We compare our calculations with proposed analytical results and inelastic neutron scattering experiments.

We use a world line quantum Monte Carlo algorithm (described in detail in [5]), based on the Suzuki-Trotter transformation [19], to calculate the imaginary-time-dependent spin correlation function, $S(\mathbf{k},\tau) = \langle S_z(\mathbf{k},\tau) \times S_z(-\mathbf{k},0)\rangle$, where $S_z(\mathbf{k},\tau) = e^{H\tau} S_z(\mathbf{k}) e^{-H\tau}$. The algorithm involves spin packing and parallelization by distributing pieces of the lattice among the nodes of a hypercube parallel processor [20]. We simulate a 64×64 quantum system at $T=0.35$, and a 32×32 system for $T>0.35$ with periodic boundary conditions. To minimize finite-size effects, the system size is kept much bigger than the correlation length ξ ($L/\xi>6$).

The dynamic structure factor $S(\mathbf{k},\omega)$ is obtained from $S(\mathbf{k},\tau)$ by inversion of the Laplace transform: $S(\mathbf{q},\tau) = (1/2\pi)\int_{-\infty}^{\infty} e^{-\omega\tau} S(\mathbf{q},\omega)\,d\omega$. For a finite set of noisy data, the inversion is ill posed. The maximum entropy method (MEM) was suggested [21] as a solution. An exhaustive account of the method may be found in [22]. It has already been successfully applied to a variety of problems (Kondo model [23], one-dimensional Heisenberg model [24], superconducting systems [25], and other problems in different fields). MEM associates prior probability $e^{\alpha I[S]}$ with a particular choice for $S(\mathbf{k},\omega)$, where the functional I is defined by

$$I = \int_0^{\infty} \left[-S(\mathbf{q},\omega) \ln \frac{S(\mathbf{q},\omega)}{m(\mathbf{q},\omega)} + S(\mathbf{q},\omega) - m(\mathbf{q},\omega) \right] d\omega .$$

The measure $m(\mathbf{k},\omega)$ is called the default model. Without Monte Carlo data, $m(\mathbf{k},\omega)$ is the outcome of the analysis. A standard χ^2 measure is used to calculate the likelihood $e^{-\chi^2/2}$ of the Monte Carlo data $S(\mathbf{k},\tau)$. The posterior probability of $S(\mathbf{k},\omega)$, given the Monte Carlo data, follows from Bayes theorem: $P \propto e^{\alpha I - \chi^2/2}$. The MEM image $S(\mathbf{k},\omega)$ maximizes this posterior probability. The parameter α, which weighs the relative importance of the misfit statistic χ^2 and entropy I, is integrated out of the problem by calculating the average $S(\mathbf{k},\omega)$, weighted by the posterior probability of α [22]. We then obtain the posterior probability $P[S]$ of the image

$S(\mathbf{k},\omega)$ given just the data and the model, which is used to pick the "best" model for a given data set. With the MEM approach we can obtain only a rough estimate of the error bars of the frequency-integrated quantities of the image [22]. The Monte Carlo (imaginary time) error bars are less than a percent at worst.

The default $m(\mathbf{k},\omega)$ is obtained by maximizing $\int_0^\infty m(\mathbf{k},\omega)\ln[m(\mathbf{k},\omega)]d\omega$, subject to the detailed balance condition $m(\mathbf{k},-\omega)=e^{-\beta\omega}m(\mathbf{k},\omega)$ and the three sum rules [26], $\int\omega^n S(\mathbf{k},\omega)d\omega=2\pi A_n(\mathbf{k})$, which are measured in the simulation: $A_{-1}=\chi(\mathbf{k})$, $A_0(\mathbf{k})=S(\mathbf{k},\tau=0)$, and $A_1(\mathbf{k})=-(\langle E\rangle/3N)[2-\cos(k_x)-\cos(k_y)]$. This sum rule (SR) default provides an excellent description of our data. We attempted to use other reasonable defaults as well. For example, the longitudinal relaxation function F^{zz}, defined by

$$S(\mathbf{k},\omega)=\frac{1}{2}\chi(\mathbf{q},T)\frac{\beta\omega}{(1-e^{-\beta\omega})}F^{zz}(\mathbf{k},\omega)\,,$$

may be approximated by a sum of Lorentzians (SL) of width $\gamma_{\mathbf{k}}$, centered at the excitation frequencies $\pm\omega_{\mathbf{k}}$. The MEM image $S(\mathbf{k},\omega)$ thus obtained deviates significantly from this default, and tends to reproduce the features obtained by SR default, i.e., broader asymmetric peaks. Also, $S(\mathbf{k},\omega)$ suggested by Auerbach and Arovas within the Schwinger boson mean field theory (SBMFT) [Eq. (6) in [8]) does not fit the data. Most importantly, the posterior probability of the images generated by SR default are 3–4 orders of magnitude bigger than by the two other defaults. Consequently, we use SR default for all further calculations. The frequency moments of the *analytically continued* $S(\mathbf{k},\omega)$ agree with static Monte Carlo data within their error bars, which is an additional check of the reliability of the MEM procedure.

The dynamic structure factor for a few points along the (π,π)-$(\pi/2,\pi/2)$ and (π,π)-$(\pi,0)$ directions is plotted in Fig. 1. The wave vector $\mathbf{q}$ is measured from the zone corner (π,π), i.e., $\mathbf{q}=\mathbf{k}-(\pi,\pi)$. The behavior of the structure factor can be well understood within a modified spin-wave picture [27]. The correlation length diverges exponentially [5] and spin waves with momenta $q\xi\geq 1$ may be well-defined excitations, because they propagate within locally ordered regions which persist on time scales longer than the short-wavelength spin-wave lifetimes. The peak in $S(\mathbf{q},\omega)$ (see inset of Fig. 1) reflects the energy and lifetime of the excitation at momentum $\mathbf{q}$. Only the longest-wavelength modes, $q\xi<1$, are sensitive to the slow variations of the local staggered magnetization. In this limit, one has diffusive spin propagation, which is reflected in broad $S(\mathbf{q},\omega)$ curves in Fig. 1. Since the staggered magnetization is not a constant of motion, the $\mathbf{q}=0$ mode appears as a quasielastic peak centered at $\omega=0$ in Fig. 1. As $T\to 0$, it turns into a true Bragg peak.

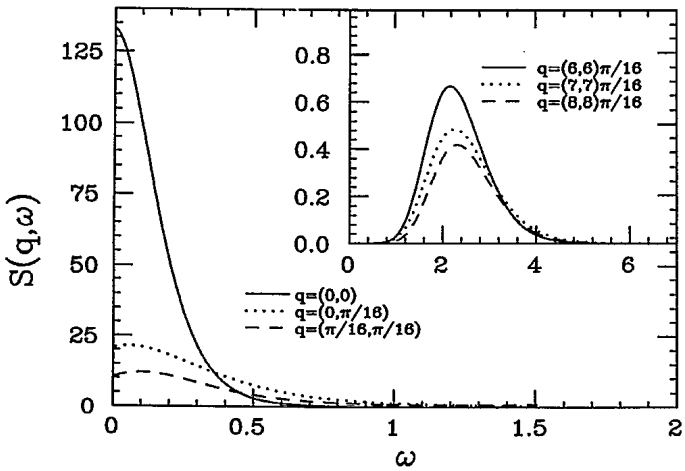

FIG. 1. The dynamic structure factor $S(\mathbf{q},\omega)$ at $T=0.38J$. In the vicinity of the antiferromagnetic vector, behavior is diffusive. Away from the zone corner (inset), $S(\mathbf{q},\omega)$ exhibits broad non-Lorentzian peaks at spin-wave frequencies.

Given that the dynamic structure factor can be qualitatively understood within the spin-wave framework, we extract the dispersion and damping of the spin waves from the moments of the longitudinal relaxation function $F^{zz}(\mathbf{q},\omega)$. The spin-wave frequency is calculated as

$$\omega_{\mathbf{q}}=\int_0^\infty \omega F^{zz}(\mathbf{q},\omega)d\omega\Big/\int_0^\infty F^{zz}(\mathbf{q},\omega)d\omega\,,$$

while the damping is obtained as $\gamma_{\mathbf{q}}^2=\langle\omega^2\rangle-\omega_{\mathbf{q}}^2$, where

$$\langle\omega^2\rangle=\int_{-\infty}^\infty \omega^2 F^{zz}(\mathbf{q},\omega)d\omega\Big/\int_{-\infty}^\infty F^{zz}(\mathbf{q},\omega)d\omega\,.$$

In Fig. 2 we show the spin-wave dispersion and linewidths at $T=0.35$. Spin-wave dispersion for higher frequencies

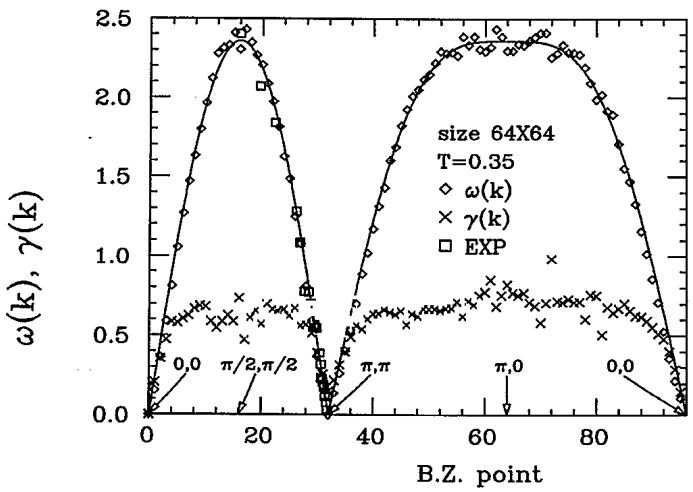

FIG. 2. Spin-wave frequencies and linewidths at $T=0.35J$. The solid line is the $T=0$ spin-wave dispersion, uniformly renormalized by the quantum factor of $Z_c=1.18$. The integers on the abscissa enumerate points in the Brillouin zone of a 64×64 system, along the triangle spanned by $\mathbf{k}_1=(0,0)$, $\mathbf{k}_2=(\pi,\pi)$, and $\mathbf{k}_3=(\pi,0)$. Calculated relative errors are of the order of 10^{-3}. The inelastic neutron scattering data (EXP) are scaled by the bare effective exchange coupling $J\simeq 0.13$ eV.

can be accurately reproduced by the $T=0$ spin-wave theory, with a *uniform* multiplicative renormalization of the spectrum coming from *quantum* renormalization of spin stiffness (or spin-wave velocity). The solid curve is the $T=0$ spectrum with spin-wave velocity renormalized by a factor of $Z_c=1.18$, as calculated by Singh and Huse and Elser [10]. This implies that the energetic spin waves are renormalized only by quantum fluctuations even at finite, but low temperatures. Longer-wavelength spin waves are softened, since the spin stiffness vanishes on length scales longer than $\xi(T)$. Our dispersion curve is in excellent agreement with recently performed inelastic neutron scattering experiments on La_2CuO_4 [28]. The experimental data, scaled by the bare exchange coupling $J\simeq 0.13$ eV [28], are also shown in Fig. 2. This value for effective exchange in CuO_2 sheets also agrees very well with our earlier estimate obtained from static spin correlations [5].

Chakravarty, Halperin, and Nelson (CHN) [7] carried out an analysis of the low-energy sector of the AFHM, based on the mapping onto the nonlinear sigma model (NLσM). Static correlations can be quantitatively understood within this framework at the two-loop level of approximation [5]. They also made a conjecture that the dynamic correlation function exhibits dynamic scaling. Our simulation shows that the model scales indeed, but the temperature dependence of the scaling frequency differs from their result.

We verified that the dynamic structure factor near $\mathbf{q}=0$ can be cast into the scaling form:

$$S(\mathbf{q},\omega)[1-\exp(-\beta\omega)]/\omega=\omega_0^{-1}S(\mathbf{q}=0)f(\mathbf{q}\xi)\times\Phi(\mathbf{q}\xi,\omega/\omega_0)\,,$$

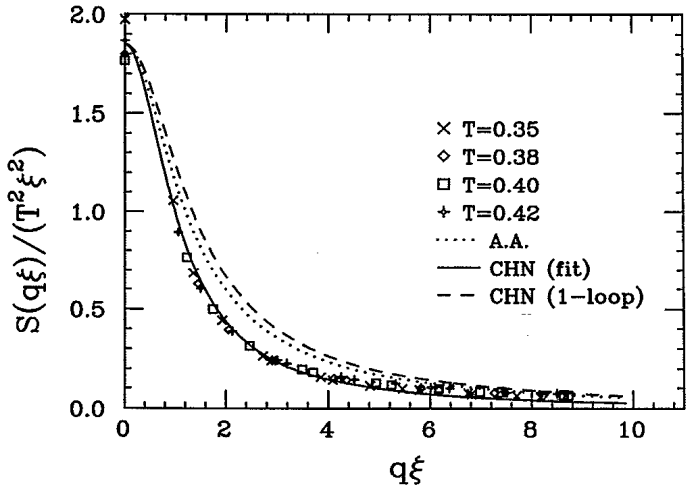

FIG. 3. The scaling plot of $f(\mathbf{q}\xi)=S(\mathbf{q})/T^2\xi^2\propto S(\mathbf{q})/S(0)$. The exact scaling function $f(x)$ disagrees with the Schwinger boson mean-field calculation (dotted line) or one-loop renormalization-group result (dashed line). When the logarithmic prefactor in the function obtained by renormalization-group analysis is reduced, the agreement is better (solid line).

TABLE I. Temperature (T), characteristic frequency scale $\omega_0(T)$, and the product of $\omega_0(T)$ and the correlation length $\xi(T)$.

T	$\omega_0(T)$	$\omega_0(T)\xi(T)$
0.35	0.184	1.81
0.38	0.243	1.80
0.40	0.289	1.81
0.42	0.308	1.67
0.45	0.378	1.68
0.50	0.450	1.51

with temperature-dependent correlation length $\xi(T)$ and frequency scale $\omega_0(T)=\gamma_{\mathbf{q}=0}$. The temperature dependence of the scaling frequency is shown in Table I. At lower temperatures, it behaves as $\omega_0\xi=$const, instead of $\omega_0\xi\propto T^{1/2}$, as conjectured by CHN. This $\omega_0\xi=$const behavior is obtained in both SBMFT [8] and modified spin-wave theory [9]. At higher temperatures, the scaling description is still valid, but the product $\omega_0\xi$ decreases, which is similar to the classical model [15].

In Fig. 3, we show the scaling plot of $S(\mathbf{q})$, assuming that $S(0)\propto T^2\xi^2$. The SBMFT result [Eq. (8) in [8]] does not agree well with our curve. The analysis based on NLσM leads to $f(x)=(1+\frac{1}{2}B_f\ln[1+x^2])/(1+x^2)$ [7]. The prefactor of the logarithm is $B_f=1$ at the one-loop level, but the one-loop curve is even further away than the mean-field result. Higher-loop corrections will change this prefactor [7] and bring the NLσM curve closer to our data. For example, the same functional form, but with $B_f\simeq 0.23$, roughly agrees with our results.

The dynamic scaling hypothesis also implies scaling for long-wavelength spin-wave frequencies, $\omega_{\mathbf{q}}=\omega_0(T)\times\Omega(\mathbf{q}\xi)$, and lifetimes, $\gamma_{\mathbf{q}}=\omega_0(T)\Gamma(\mathbf{q}\xi)$ [16]. In Fig. 4, we show the scaling plots of $\omega_{\mathbf{q}}$ and $\gamma_{\mathbf{q}}$. At low frequen-

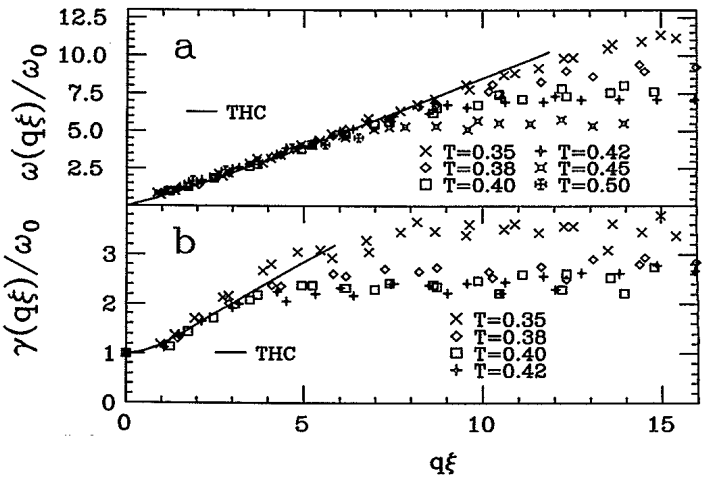

FIG. 4. (a) The scaling plot of spin-wave frequencies $\omega_{\mathbf{q}}=\omega_0(T)\Omega(\mathbf{q}\xi)$. (b) The scaling plot of spin-wave linewidths $\gamma_{\mathbf{q}}=\omega_0(T)\Gamma(\mathbf{q}\xi)$. The solid lines correspond to the scaling functions proposed in Ref. [16].

cies and momenta, data from different temperatures collapse onto the same curve (the scatter in γ_q is somewhat bigger than for the dispersion). We also plot the scaling functions $\Omega(x)=\sqrt{3/2}x[\delta+\frac{1}{2}A\ln(1+x^2)]^{1/2}$ and $\Gamma(x)=[1+\mu x^2]/[1+\theta\ln(1+x^2)]^{3/2}$, proposed in Ref. [16]. The following choice of parameters yields a reasonably good agreement with our data: $\delta=0.25$, $A=0.1$, $\mu=0.85$, and $\theta=0.23$. The prefactor A is equal to 1 in the renormalization-group analysis [16]. It is not possible to fit the data with the $A=1$ curve, for any value of δ. It is likely that higher-loop corrections will lower this parameter, just like B_f in the expression for the scaling function $f(x)$. With the present quality of the data for damping we obtain qualitative agreement with $\Gamma(x)$ proposed in [16].

To summarize, we used a combination of quantum Monte Carlo and maximum entropy methods to compute the dynamic correlation function $S(\mathbf{q},\omega)$ of the isotropic quantum Heisenberg antiferromagnet at low temperatures, on square lattices of up to 64×64 spins. We show that the dynamics can be understood within the framework of renormalized damped spin waves. High-frequency excitations in the low-temperature limit are uniformly renormalized by quantum fluctuations only. The multiplicative renormalization factor for the spin-wave velocity is very accurately given by the series expansion result $Z_c=1.18$ [10]. These conclusions are in excellent agreement with inelastic neutron scattering experiments on La_2CuO_4. The long-wavelength and low-energy sector exhibits scaling behavior. Our results are consistent with the dynamic scaling theory based on a combination of the renormalization-group analysis, hydrodynamics, and model calculations [3]. The only qualitative discrepancy is the temperature dependence of the characteristic frequency scale, which follows an $\omega_0\propto\xi^{-1}$ behavior at low temperatures.

The authors gratefully acknowledge valuable interactions with D. L. Cox, M. C. Cross, G. C. Fox, P. B. Weichman, J. Deisz, J. W. Wilkins, and R. McKenzie. This work is supported by NSF Grants No. ASC-9015000, No. DMR-8857341, No. DMR-8715474, and No. DMR-9107563. We are also thankful for a generous allottment of computer time on Caltech/JPL MarkIIIfp hypercubes at The Caltech Concurrent Computation Project and on the Cray-YMP at The Ohio Supercomputer Center.

[1] J. G. Bednorz and K. A. Müller, Z. Phys. B **64**, 189 (1986).
[2] P. W. Anderson, Science **235**, 1196 (1987).
[3] E. Manousakis, Rev. Mod. Phys. **63**, 1 (1991).
[4] G. Aeppli *et al.*, Phys. Rev. Lett. **62**, 2052 (1989).
[5] H. Q. Ding and M. S. Makivić, Phys. Rev. Lett. **64**, 1449 (1990).
[6] R. R. P. Singh, P. A. Fleury, K. B. Lyons, and P. E. Sulewski, Phys. Rev. Lett. **62**, 2736 (1989).
[7] S. Chakravarty, B. I. Halperin, and D. Nelson, Phys. Rev. Lett. **60**, 1057 (1988); Phys. Rev. B **39**, 2344 (1989).
[8] A. Auerbach and D. P. Arovas, Phys. Rev. Lett. **61**, 617 (1988).
[9] M. Takahashi, Phys. Rev. Lett. **58**, 168 (1987); Prog. Theor. Phys. Suppl. **101**, 487 (1990).
[10] R. R. P. Singh, Phys. Rev. B **39**, 9760 (1989); D. A. Huse and V. Elser, Phys. Rev. Lett. **60**, 2531 (1988).
[11] Y. Okabe and M. Kikuchi, J. Phys. Soc. Jpn. **57**, 4351 (1988); S. Miyashita, J. Phys. Soc. Jpn. **57**, 1934 (1988).
[12] G. Gomez-Santos, J. D. Joannopoulos, and J. W. Negele, Phys. Rev. B **39**, 4435 (1989).
[13] S. Liang, Phys. Rev. B **42**, 6555 (1990).
[14] J. D. Reger and A. P. Young, Phys. Rev. B **37**, 5978 (1988); M. Gross, E. Sanchez-Velasco, and E. Siggia, Phys. Rev. B **39**, 2484 (1989); N. Trivedi and D. Ceperley, Phys. Rev. B **40**, 2737 (1989).
[15] G. M. Wysin and A. R. Bishop, Phys. Rev. B **42**, 810 (1990).
[16] S. Tyc, B. I. Halperin, and S. Chakravarty, Phys. Rev. Lett. **62**, 835 (1989); S. Tyc and B. Halperin, Phys. Rev. B **42**, 2096 (1990).
[17] T. Becher and G. Reiter, Phys. Rev. Lett. **63**, 1004 (1989).
[18] C.-X. Chen and H.-B. Schutler, Phys. Rev. B **40**, 2096 (1989).
[19] M. Suzuki, Prog. Theor. Phys. **56**, 1457 (1976).
[20] G. C. Fox, Concurrency: Practice and Experience **1**, 63 (1989).
[21] R. N. Silver, D. S. Sivia, and J. E. Gubernatis, Phys. Rev. B **41**, 2380 (1990).
[22] J. E. Gubernatis, M. Jarrell, R. N. Silver, and D. S. Sivia, Phys. Rev. B **44**, 6011 (1991).
[23] R. N. Silver, J. E. Gubernatis, D. S. Sivia, and M. Jarrell, Phys. Rev. Lett. **65**, 496 (1990); M. Jarrell, J. E. Gubernatis, R. N. Silver, and D. S. Sivia, Phys. Rev. B **43**, 1206 (1991).
[24] J. Deisz, M. Jarrell, and D. Cox, Phys. Rev. B **42**, 4869 (1990).
[25] M. Jarrell, D. S. Sivia, and B. Patton, Phys. Rev. B **42**, 4804 (1990).
[26] P. C. Hohenberg and W. F. Brinkman, Phys. Rev. B **10**, 128 (1974).
[27] F. B. McLean and M. Blume, Phys. Rev. B **7**, 1149 (1973).
[28] S. M. Hayden *et al.*, Phys. Rev. Lett. **67**, 3622 (1991).